



CHORUS

This is the accepted manuscript made available via CHORUS. The article has been published as:

Gate Tuning of Electronic Phase Transitions in Two-Dimensional NbSe₂

Xiaoxiang Xi, Helmuth Berger, László Forró, Jie Shan, and Kin Fai Mak

Phys. Rev. Lett. **117**, 106801 — Published 29 August 2016

DOI: [10.1103/PhysRevLett.117.106801](https://doi.org/10.1103/PhysRevLett.117.106801)

Gate tuning of electronic phase transitions in two-dimensional NbSe₂

Xiaoxiang Xi¹, Helmuth Berger², László Forró², Jie Shan^{1*}, and Kin Fai Mak^{1*}

¹Department of Physics and Center for 2-Dimensional and Layered Materials, The Pennsylvania State University, University Park, Pennsylvania 16802-6300, USA

²Institute of Condensed Matter Physics, Ecole Polytechnique Fédérale de Lausanne, 1015 Lausanne, Switzerland

*Correspondence to: jus59@psu.edu (J.S.), kzm11@psu.edu (K.F.M.)

Abstract

Recent experimental advances in atomically thin transition metal dichalcogenide (TMD) metals have unveiled a range of interesting phenomena including the coexistence of charge-density-wave (CDW) order and superconductivity down to the monolayer limit. The atomic thickness of two-dimensional (2D) TMD metals also opens up the possibility for control of these electronic phase transitions by electrostatic gating. Here, we demonstrate reversible tuning of superconductivity and CDW order in model 2D TMD metal NbSe₂ by an ionic liquid gate. A variation up to ~ 50% in the superconducting transition temperature has been observed. Both superconductivity and CDW order can be strengthened (weakened) by increasing (reducing) the carrier density in 2D NbSe₂. The doping dependence of these phase transitions can be understood as driven by a varying electron-phonon coupling strength induced by the gate-modulated carrier density and the electronic density of states near the Fermi surface.

In metals, the interactions between free carriers and ions that form the crystal structure lead to a multitude of many-body electronic phases [1]. Modifying the free carrier density, and thus the density of states (DOS) near the Fermi surface and screening of the interactions, has long been sought to control the electronic phases [2]. Electrostatic gating is a clean and reversible method to introduce doping near the surface of a material [3]. In particular, electric-double-layer based on an ionic liquid has had a tremendous success in doping various insulator surfaces into metallic phases [4-15]. However, little success has been made on significantly changing the carrier density in metals by electrostatic gating due to screening arisen from the extremely high carrier densities [16-18]. Recent experimental advances in atomically thin transition metal dichalcogenide (TMD) metals have unveiled a range of interesting collective electronic phenomena, including the coexistence of charge-density-wave (CDW) order and superconductivity down to the monolayer limit [19-21], a Bose metal phase [22], and Ising pairing in superconductivity [23]. The atomic thickness of two-dimensional (2D) TMD metals has also provided an ideal system to explore electrostatic doping and control of the collective electronic phases in the high-density metallic regime, where the high electronic DOS leads to multiple electronic instabilities.

2H-NbSe₂ is a representative TMD metal made of layers bonded by van der Waals' interactions [24]. Each single NbSe₂ layer (half of a unit cell thickness) consists of a layer of transition metal Nb atoms sandwiched between two layers of chalcogen Se atoms, forming a trigonal prismatic structure. The electronic band structure near the Fermi surface shows multiple pockets formed by the valence Bloch states [Fig. 1(a) for bilayer NbSe₂] [25]. 2H-NbSe₂ is a hole metal at room temperature. It undergoes a CDW and superconducting transition, respectively, at ~ 33 and 7 K in the bulk, with the two collective phases coexisting below 7 K [24]. Because of the weak interlayer van der Waals' bonding, NbSe₂ has been successfully exfoliated into atomically thin layers [19,20,22,23,26,27]. Monolayer NbSe₂ has also been grown on graphene by molecular beam epitaxy (MBE) [21]. With decreasing layer thickness, whereas all studies consistently show a decreasing superconducting transition temperature T_{C0} , detailed values vary among samples of different origin [19-23]. A large discrepancy also exists in the reported CDW transition temperature T_{CDW} . For instance, Xi et al. observed strongly enhanced CDW order in atomically thin NbSe₂ with $T_{CDW} > 100$ K for exfoliated monolayer samples [19]. Ugeda et al. reported slightly weakened CDW order ($T_{CDW} \sim 25$ K) in monolayer NbSe₂ grown on graphene [21]. These discrepancies are not well understood although sample quality and substrates are believed to play a role.

In this Letter, we employ transport and magnetotransport measurements to investigate the superconducting and CDW phase transition in 2D NbSe₂ as a function of carrier density modulated by ionic liquid gating. We have been able to *reversibly* tune the carrier density in bilayer NbSe₂ by up to 6×10^{14} cm⁻² ($\sim 30\%$ of the intrinsic density), and the superconducting transition temperature by $\sim 50\%$, with enhanced (weakened) T_{C0} for hole (electron) doping. Although the precise value of T_{CDW} cannot be determined, similar trend with doping has been observed. The observed doping dependence of the

superconducting and CDW transition can be understood as a result of electron-phonon (*e-ph*) coupling modulated by the carrier density and the corresponding electronic DOS near the Fermi surface. Our results show that unintentional doping could contribute to the discrepancies among the reported critical temperatures. In contrast to previous studies on gate-induced superconductivity in electron-doped MoS₂ [8,10,11,15], our work focuses on a high-density hole-doped regime, in which the Fermi level is located near the middle of the valence bands [Fig. 1(a)] with a much higher electronic DOS and stronger spin-orbit interactions. We also note that while pressure tuning of the CDW and superconducting transitions in bulk NbSe₂ has been demonstrated [28-30], our study examines continuous electrical tuning of these transitions in 2D NbSe₂ over a large window of doping densities, which is not accessible in bulk metallic materials.

Atomically thin NbSe₂ is known to be unstable under ambient conditions [19,20,22,23,27]. In fact, recent advances on the study of its intrinsic properties have been made possible only by capping NbSe₂ [19,20,22,23] or performing in-situ measurements [21]. In recent gating studies of relatively thick NbSe₂ flakes using an ionic liquid [31,32], NbSe₂ flakes were brought into direct contact with the ionic liquid and an irreversible behavior was observed at high gate voltages. This is presumably caused by electrochemistry on the surfaces of NbSe₂. To protect the 2D NbSe₂ samples from oxidation and undesired electrochemistry in ionic liquid gating while maintaining the high gate capacitance of the device, we have introduced an ultrathin capping layer of a chemically stable large-gap semiconductor [33,34] or insulator [13,14]. Both MoS₂ monolayers and ultrathin (~ 1 nm) hexagonal boron nitride (hBN) layers have been tested. Within the gate voltage range of interest, they have produced similar results (Supplementary Section 1 [35]). We have mainly used monolayer MoS₂ since it is much easier to identify than ultrathin hBN based on optical reflectance in the visible.

The fabrication method of 2D NbSe₂ devices has been described elsewhere [23]. In brief, atomically thin NbSe₂ samples were mechanically exfoliated from bulk single crystals on silicone elastomer polydimethylsiloxane (PDMS) substrates. Their thickness was first identified by the optical reflectance contrast and later confirmed by Raman spectroscopy [19]. The samples were then transferred onto silicon substrates with pre-patterned Au electrodes and shaped into a Hall bar geometry by removing unwanted areas using a polypropylene carbonate (PPC) layer on a PDMS stamp. Capping layers prepared on separate substrates were subsequently transferred onto NbSe₂. Ionic liquid *N,N*-diethyl-*N*-(2-methoxyethyl)-*N*-methylammonium bis(trifluoromethylsulphonylimide) (DEME-TFSI) was finally drop casted, covering both the sample and the gate electrode. The schematic and optical microscope image of a typical device are shown in Fig. 1(b) & 1(c), respectively. The finished devices were annealed at 350 K in high vacuum for 3 – 5 hours to dehydrate the ionic liquid and to ensure good interfacial contacts between different layers. Since it is much easier to fabricate high-quality bilayer than monolayer devices, we focus our study on NbSe₂ bilayers. Similar results but stronger effects are expected for monolayers.

Transport measurements were carried out in a Physical Property Measurement System down to 2.1 K. Both longitudinal sheet resistance (R_s) and transverse sheet resistance (R_t) were acquired with excitation currents limited to 1 μ A to avoid heating and high-bias effects. Because of the finite longitudinal-transverse coupling in our devices and the presence of magnetoresistance at low temperature, we antisymmetrized the transverse sheet resistance under magnetic field H of opposite directions to obtain the Hall resistance, $R_{xy}(H) = \frac{R_t(H) - R_t(-H)}{2}$, and the sheet Hall coefficient, $R_H = \frac{R_{xy}}{H}$. (See Supplementary Section 2 for more details [35].) To vary the doping density, gate voltage was adjusted at 220 K (which is near the freezing point of the ionic liquid [8]), followed by rapid cooling to minimize any electrochemistry effects.

Figure 2 shows the temperature dependence of the sheet resistance R_s under zero magnetic field and the sheet Hall coefficient R_H of a typical device (#120) under gate voltage V_G varying from -2 V to 3 V. Metallic behavior is seen in the temperature dependence of R_s [Fig. 2(a)]: R_s scales linearly with temperature T due to e - ph scattering at high temperature, and saturates to a residual value of about 250 Ω due to impurity/defect scattering at low temperature. The residual-resistance ratio (RRR) (estimated as $\frac{R_s(300K)}{R_s(8K)}$) is about 6. Further cooling causes a rapid drop of R_s to zero below 5 K, indicating a superconducting transition. Fig. 2(b) clearly shows that T_{C0} shifts by \sim 30% under gate voltage varying from -2 V to 3 V. This modification is in contrast to previous experiments based on silicon or oxide back gates, where very small modulations in T_{C0} (< 0.2 K) have been reported [20,27,36]. Similarly, R_H also depends strongly on gate voltage [Fig. 2(c)]: for $T > 100$ K, R_H is largely temperature independent; its value increases with increasing V_G . For $T < 100$ K, a drop in R_H upon cooling is observed under V_G up to ~ 2 V; the drop in R_H eventually turns into a rise under large positive V_G 's. As we discuss below, the high-temperature behavior of R_H is dominated by the carrier density and will be used to evaluate its value; and the low-temperature behavior is influenced by the CDW transition.

Before we interpret the above results, we perform multiple control experiments. (See Supplementary Section 1 for details [35].) First we test the reversibility of the effect. Six bilayer devices have been tested under different gating sequences. All of them were highly reversible and repeatable under the gate voltage range of -2 V to 3 V. (Some devices withstood higher gate voltages, e.g. #150.) Thus extrinsic effects such as gate-induced electrochemistry are unlikely the origin of the observed effects. Second, we compare ionic liquid gating with conventional solid-state dielectric gating by fabricating a bilayer NbSe₂ device with a combination of a Si/SiO₂ back gate and a graphene/hBN top gate. Similar effects on T_{C0} , but much smaller modulations, have been observed. Third, we verify the role of the MoS₂ capping layer. To exclude the possibility of gate-induced superconductivity in MoS₂, as has been recently demonstrated [8,10,11,15], we have performed an identical experiment on monolayer MoS₂ alone. No gate-induced superconductivity was observed within the gate voltage range employed in this work. The

MoS₂ film thus only serves as a protection layer similar to ultrathin hBN. Finally we note that in addition to doping, electrostatic gating with a single gate also introduces a vertical electric field on the samples. The device with dual solid-state gates showed that the electric-field effect on the electronic phase transitions is negligible compared to the doping effect. We therefore only consider the doping effects in NbSe₂ below.

We now extract the doping dependence of the superconducting transition temperature of bilayer NbSe₂. For simplicity, we have taken T_{C0} to be the temperature corresponding to half of the normal state resistance (see Supplementary Section 3 for more accurate determinations of T_{C0} and for current excitation measurements at varying temperatures [35]). To extract the total sheet density n_{2D} , we have used the high-temperature (> 100 K) value of the Hall coefficient R_H . Although NbSe₂ is a multiband metal, it has been shown that at high temperature the carrier scattering rate becomes isotropic in the Fermi surface and R_H can provide a good estimate of the carrier density by using $n_{2D} = \frac{f}{eR_H}$ [37]. Here e is the elementary charge, and f is a dimensionless parameter close to unity. A value of $f \approx 0.8$ has been obtained by calibrating n_{2D} at $V_G = 0$ V to the known carrier density n_0 in bulk NbSe₂: $n_{2D} = n_0 t \approx 1.9 \times 10^{15} \text{cm}^{-2}$ ($n_0 \approx 1.5 \times 10^{22} \text{cm}^{-3}$ corresponds to 1 hole per Nb atom and $t \approx 1.25$ nm is the bilayer thickness [24]). We note that in the above calibration we have ignored charge transfer between MoS₂ and NbSe₂ due to their work function mismatch, which has been estimated $< 10^{13} \text{cm}^{-2}$. The V_G -dependence of n_{2D} is shown in Fig. 2(d) (symbols), which follows a linear dependence (dashed line). The negative slope is consistent with the fact that NbSe₂ is a hole metal. We calculate the gate capacitance from the slope to be $7 \mu\text{F}/\text{cm}^2$. The value agrees very well with the reported ones for the same ionic liquid [8]. The corresponding tuning range of the Fermi energy, calibrated from the DOS at the Fermi surface from *ab initio* calculations [25], is ~ 130 meV [shaded region in the electronic band structure of Fig. 1(a)].

Figure 3(a) summarizes the doping dependence of T_{C0} for three bilayer devices. It clearly shows a monotonic dependence of T_{C0} on (hole) density and the ability of gate tuning of T_{C0} from 2.8 K to 5.2 K (4.5 K for undoped case), which correspond to a modulation of $\sim 50\%$. In Fig. 3(b) we show the perpendicular critical field ($H_{C2\perp}$) - critical temperature (T_C) phase diagram at different doping levels. Following the same convention used for zero magnetic field, we have determined T_C at half of the normal state resistance. We note that the $H_{C2\perp} - T_C$ phase diagram is complicated by the enhanced vortex fluctuation effects in 2D, giving rise to much broadened superconducting transitions under finite magnetic fields (see Supplementary Section 4 [35]) [22,38]. Near T_{C0} , the $H_{C2\perp} - T_C$ dependences are well described by a linear

relation $H_{C2\perp} = \frac{\Phi_0}{2\pi\xi_0^2} (1 - \frac{T_C}{T_{C0}})$ (solid lines), where Φ_0 and ξ_0 denote the flux quantum and the superconducting coherence length, respectively [22,38]. The magnitude of the slope increases with increasing T_{C0} , from which the superconducting coherent length ξ_0

can be determined to decrease with T_{C0} , equivalently, also with the hole density [inset, Fig. 3(b)]. Furthermore, the increasing slope also projects a higher upper critical field (at $T = 0$) with increasing T_{C0} [38]. This finding in bilayer NbSe₂ is distinct from that in bulk NbSe₂ under high pressure, where the upper critical field has been observed to decrease with increasing T_{C0} [29]. We note that unlike the anomalous behavior under high pressure that requires a complete two-band model to understand, superconductivity in bulk NbSe₂ under low pressure can be described by a simple one-band approximation since *e-ph* coupling in one of the bands dominates [29]. Below we compare our experiment to the simple one-band model.

Superconductivity in bulk NbSe₂ is known to be the BCS type driven by *e-ph* interactions. In the one-band model, T_{C0} is predicted by the strong-coupling formula as [39]

$$T_{C0} = \frac{\omega_{log}}{1.2} \exp \left[-\frac{1.04(1+\lambda)}{\lambda - \mu^*(1+0.62\lambda)} \right]. \quad (1)$$

Here ω_{log} is the weighted average of the phonon energies in Kelvin introduced by Allen and Dynes [39], μ^* is the Coulomb pseudopotential, and $\lambda = N(\epsilon_F)V_0$ is the dimensionless *e-ph* coupling constant with $N(\epsilon_F)$ and V_0 denoting, respectively, the electronic DOS at the Fermi energy ϵ_F and the effective *e-ph* coupling energy V_0 . We evaluate the dimensionless *e-ph* coupling constant λ from the temperature dependence of the longitudinal resistance, specifically its slope $\frac{dR_s}{dT}$ at high temperature [Fig. 2(a)]. Electron-phonon scattering in a 2D metal leads to $\frac{dR_s}{dT} = \frac{2\pi\hbar n_0 k_B}{\epsilon_0 n_{2D} (\hbar\omega_{p0})^2} \lambda$, where \hbar , k_B , ϵ_0 and $\hbar\omega_{p0}$ (≈ 2.74 eV [40]) are the Planck's constant, Boltzmann constant, vacuum permittivity, and the in-plane plasma energy of bulk NbSe₂, respectively [1]. (See Supplementary Section 5 for details [35]). The dependence of λ on carrier density n_{2D} is shown in Fig. 4(a). The dependence of T_{C0} on λ is shown in Fig. 4(b) (symbols). The latter can be reasonably well described by Eq. (1) with $\omega_{log} \approx 50$ K and $\mu^* \approx 0.10$ (solid line). The value of ω_{log} agrees well with the reported one from the layer thickness dependence of T_{C0} for 2D NbSe₂ [23]. The value of μ^* is consistent with the estimate $\mu^* \approx \frac{0.26N(\epsilon_F)}{1+N(\epsilon_F)} \approx 0.15$ [41] from the DOS at the Fermi energy from *ab initio* calculations for undoped NbSe₂ [25].

Finally, we comment on the CDW order in 2D NbSe₂. A kink in the longitudinal resistance R_s and a drop (even a change of sign for high-quality samples) in the Hall coefficient R_H around T_{CDW} upon cooling due to Fermi surface instability [42,43] have been established and widely used as the transport signature of the CDW transition in bulk isoelectronic group-V TMDs (2H-NbSe₂, TaSe₂, NbS₂, and TaS₂) [30,44]. Among these compounds, NbS₂ is known not to possess a CDW phase and its Hall coefficient shows a rise instead of a drop upon cooling [empty triangles, Fig. 2(c)] [24,44]; and TaSe₂ is

known to possess strong CDW signature in transport [30,44]. We have performed a doping dependence study of the CDW transition in both bilayer NbSe₂ (Fig. 2) and TaSe₂ (Supplementary Section 6 [35]). In the latter the strong CDW transition signature has allowed us to determine T_{CDW} and conclude that the CDW order is weakened with increasing V_G (decreasing hole density). In NbSe₂, the kink in R_S is significantly broadened and cannot be identified [Fig. 2(a)] presumably due to the sample's low RRRs. A drop in R_H is still observed for V_G up to ~ 2 V, but the amount of the drop decreases with V_G till reaching ~ 3 V, at which R_H increases monotonically upon cooling as observed in NbS₂ [Fig. 2(c)]. These observations provide strong evidence that the CDW order in bilayer NbSe₂ is also weakened with decreasing hole density and can potentially even be destroyed at large gate voltages.

The correlated dependence of superconductivity and CDW order on doping observed in our experiment suggests a peaceful coexistence of the two orders in 2D NbSe₂, in accord with the behavior in bulk NbSe₂ and related TMDs revealed by recent high-pressure studies [29,30]. Angle-resolved photoemission spectroscopy (ARPES) [45] shows that while anisotropic s-wave superconducting gaps are opened at the NbSe₂ Fermi surface, CDW gaps are opened only near the CDW wavevectors, where the superconducting gap is minimum; the two orders thus have minimum effects on each other. The influence of the anisotropic CDW gap on the superconducting gap has also been investigated by scanning tunneling microscopy (STM) experiments [46]. Future studies on 2D NbSe₂ or similar systems by introducing higher hole doping densities so that the Fermi level approaches the saddle point singularity at the M-point of the Brillouin zone [25] would be very interesting. It may lead to drastic changes and even new phenomena in the collective electronic phases such as a superconducting dome observed recently in heavily doped MoS₂ [8].

Acknowledgement

The experimental research was supported by the National Science Foundation through Grant No. DMR-1645901 (sample and device fabrication), DMR-1410407 (optical characterization) and the Air Force Office of Scientific Research under grant FA9550-16-1-0249 (transport measurements). Support for data analysis was provided by the US Department of Energy, Office of Basic Energy Sciences contract No. DESC0012635 (J.S.) and No. DESC0013883 (K.F.M.). The work in Lausanne was supported by the Swiss National Science Foundation.

References

- [1] G. Grimvall, *The Electron-Phonon Interaction in Metals* (North-Holland Publishing Co., 1981).
- [2] R. E. Glover and M. D. Sherrill, *Physical Review Letters* **5**, 248 (1960).
- [3] C. H. Ahn *et al.*, *Reviews of Modern Physics* **78**, 1185 (2006).

- [4] K. Ueno, S. Nakamura, H. Shimotani, A. Ohtomo, N. Kimura, T. Nojima, H. Aoki, Y. Iwasa, and M. Kawasaki, *Nat Mater* **7**, 855 (2008).
- [5] A. T. Bollinger, G. Dubuis, J. Yoon, D. Pavuna, J. Misewich, and I. Bozovic, *Nature* **472**, 458 (2011).
- [6] Y. Lee, C. Clement, J. Hellerstedt, J. Kinney, L. Kinnischtzke, X. Leng, S. D. Snyder, and A. M. Goldman, *Physical Review Letters* **106**, 136809 (2011).
- [7] X. Leng, J. Garcia-Barriocanal, S. Bose, Y. Lee, and A. M. Goldman, *Physical Review Letters* **107**, 027001 (2011).
- [8] J. T. Ye, Y. J. Zhang, R. Akashi, M. S. Bahramy, R. Arita, and Y. Iwasa, *Science* **338**, 1193 (2012).
- [9] M. Yoshida, Y. Zhang, J. Ye, R. Suzuki, Y. Imai, S. Kimura, A. Fujiwara, and Y. Iwasa, *Scientific Reports* **4**, 7302 (2014).
- [10] Y. Saito *et al.*, *Nat Phys* **12**, 144 (2016).
- [11] J. M. Lu, O. Zheliuk, I. Leermakers, N. F. Q. Yuan, U. Zeitler, K. T. Law, and J. T. Ye, *Science* **350**, 1353 (2015).
- [12] Y. J. Yu *et al.*, *Nature Nanotechnology* **10**, 270 (2015).
- [13] L. J. Li, E. C. T. O'Farrell, K. P. Loh, G. Eda, B. Özyilmaz, and A. H. Castro Neto, *Nature* **529**, 185 (2016).
- [14] P. Gallagher, M. Lee, T. A. Petach, S. W. Stanwyck, J. R. Williams, K. Watanabe, T. Taniguchi, and D. Goldhaber-Gordon, *Nat Commun* **6**, 6437 (2015).
- [15] D. Costanzo, S. Jo, H. Berger, and A. F. Morpurgo, *Nat Nano* **11**, 339 (2016).
- [16] J. Choi, R. Pradheesh, H. Kim, H. Im, Y. Chong, and D.-H. Chae, *Applied Physics Letters* **105**, 012601 (2014).
- [17] M. Sagmeister, U. Brossmann, S. Landgraf, and R. Würschum, *Physical Review Letters* **96**, 156601 (2006).
- [18] T. A. Petach, M. Lee, R. C. Davis, A. Mehta, and D. Goldhaber-Gordon, *Physical Review B* **90**, 081108 (2014).
- [19] X. Xi, L. Zhao, Z. Wang, H. Berger, L. Forró, J. Shan, and K. F. Mak, *Nature Nanotechnology* **10**, 765 (2015).
- [20] Y. Cao *et al.*, *Nano Letters* **15**, 4914 (2015).
- [21] M. M. Ugeda *et al.*, *Nat Phys* **12**, 92 (2015).
- [22] A. W. Tsen *et al.*, *Nat Phys* **12**, 208 (2016).
- [23] X. Xi, Z. Wang, W. Zhao, J.-H. Park, K. T. Law, H. Berger, L. Forro, J. Shan, and K. F. Mak, *Nat Phys* **12**, 139 (2016).
- [24] J. A. Wilson, F. J. Di Salvo, and S. Mahajan, *Adv Phys* **50**, 1171 (2001).
- [25] M. Calandra, I. I. Mazin, and F. Mauri, *Physical Review B* **80**, 241108 (2009).
- [26] R. F. Frindt, *Physical Review Letters* **28**, 299 (1972).
- [27] N. E. Staley, J. Wu, P. Eklund, Y. Liu, L. J. Li, and Z. Xu, *Physical Review B* **80**, 184505 (2009).
- [28] C. W. Chu, V. Diatschenko, C. Y. Huang, and F. J. DiSalvo, *Physical Review B* **15**, 1340 (1977).
- [29] H. Suderow, V. G. Tissen, J. P. Brison, J. L. Martinez, and S. Vieira, *Physical Review Letters* **95**, 117006, 117006 (2005).
- [30] D. C. Freitas *et al.*, *Physical Review B* **93**, 184512, 184512 (2016).
- [31] Z. J. Li, B. F. Gao, J. L. Zhao, X. M. Xie, and M. H. Jiang, *Superconductor Science and Technology* **27**, 015004 (2014).

- [32] M. Yoshida, J. Ye, T. Nishizaki, N. Kobayashi, and Y. Iwasa, *Applied Physics Letters* **108**, 202602 (2016).
- [33] K. F. Mak, C. Lee, J. Hone, J. Shan, and T. F. Heinz, *Physical Review Letters* **105** (2010).
- [34] A. Splendiani, L. Sun, Y. Zhang, T. Li, J. Kim, C.-Y. Chim, G. Galli, and F. Wang, *Nano Letters* **10**, 1271 (2010).
- [35] See Supplemental Material [url], which includes Refs. [1,24,38,40,44,47-49].
- [36] S. E.-B. Mohammed, W. Daniel, R. Saverio, B. Geetha, P. Don Mck, and J. B. Simon, *Superconductor Science and Technology* **26**, 125020 (2013).
- [37] N. P. Ong, *Physical Review B* **43**, 193 (1991).
- [38] M. Tinkham, *Introduction to superconductivity* (McGraw-Hill, United States of America, 1996), 2nd edn.
- [39] P. B. Allen and R. C. Dynes, *Physical Review B* **12**, 905 (1975).
- [40] S. V. Dordevic, D. N. Basov, R. C. Dynes, and E. Bucher, *Physical Review B* **64**, 161103 (2001).
- [41] K. H. Benneman and J. W. Garland, *Superconductivity in d- and f-band metals* (American Institute of Physics, 1972), p. 103.
- [42] R. Bel, K. Behnia, and H. Berger, *Physical Review Letters* **91**, 066602 (2003).
- [43] L. Li, J. Shen, Z. Xu, and H. Wang, *International Journal of Modern Physics B* **19**, 275 (2005).
- [44] M. Naito and S. Tanaka, *Journal of the Physical Society of Japan* **51**, 219 (1982).
- [45] D. J. Rahn, S. Hellmann, M. Kalläne, C. Sohrt, T. K. Kim, L. Kipp, and K. Rossnagel, *Physical Review B* **85**, 224532 (2012).
- [46] I. Guillamon, H. Suderow, S. Vieira, L. Cario, P. Diener, and P. Rodiere, *Physical Review Letters* **101**, 166407, 166407 (2008).
- [47] T. Kumakura, H. Tan, T. Handa, M. Morishita, and H. Fukuyama, *Czech J Phys* **46**, 2611 (1996).
- [48] M. R. Beasley, J. E. Mooij, and T. P. Orlando, *Physical Review Letters* **42**, 1165 (1979).
- [49] L. G. Aslamasov and A. I. Larkin, *Physics Letters A* **26**, 238 (1968).

Figures and figure captions

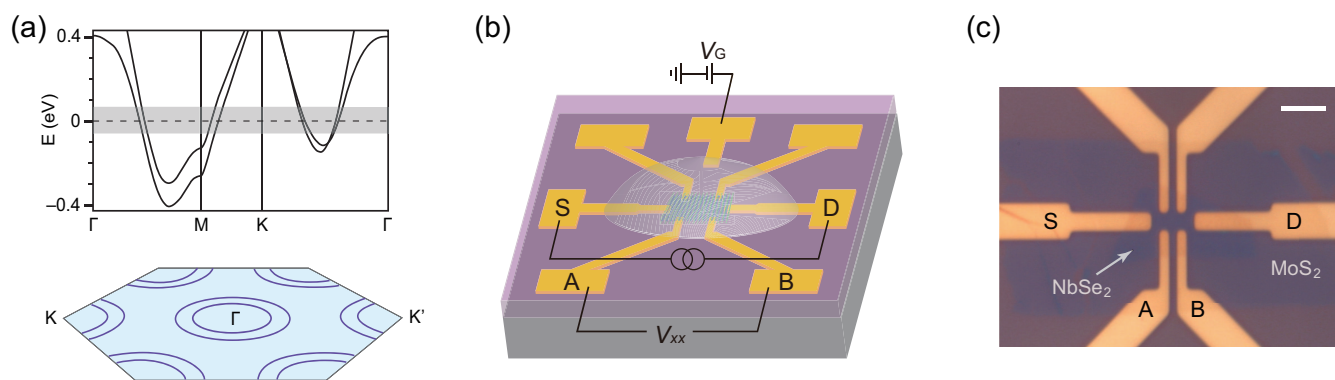
FIG. 1. (a) Top: Electronic band structure of undoped bilayer NbSe₂ reproduced from *ab initio* calculations of Ref [25]. The dashed line indicates the Fermi level at zero gate voltage and the shaded region represents the range of Fermi levels accessible by gating in our experiment. Bottom: Schematic of the first Brillouin zone and the Fermi surface around the Γ , K, and K' point. (b) Device schematic: Current was excited through electrode S and D; Longitudinal and transverse voltage drops were measured; Gate voltage V_G was supplied through an isolated electrode from the sample. (c) Optical image of a bilayer NbSe₂/monolayer MoS₂ stack on a Si substrate with gold electrodes before drop casting the ionic liquid. Scale bar is 5 μ m.

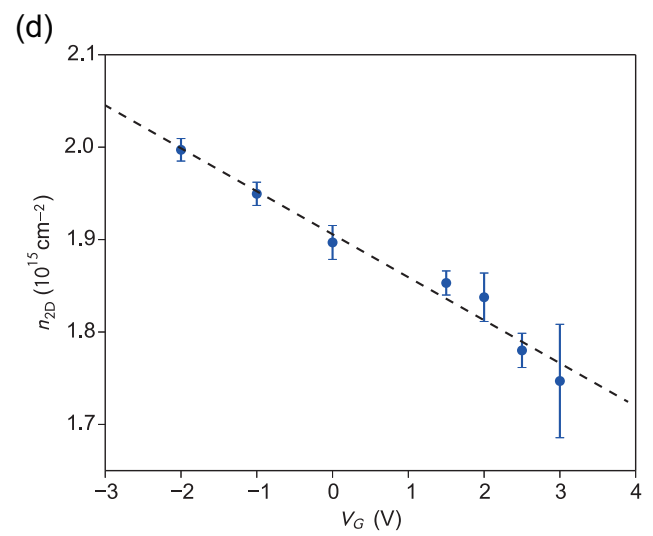
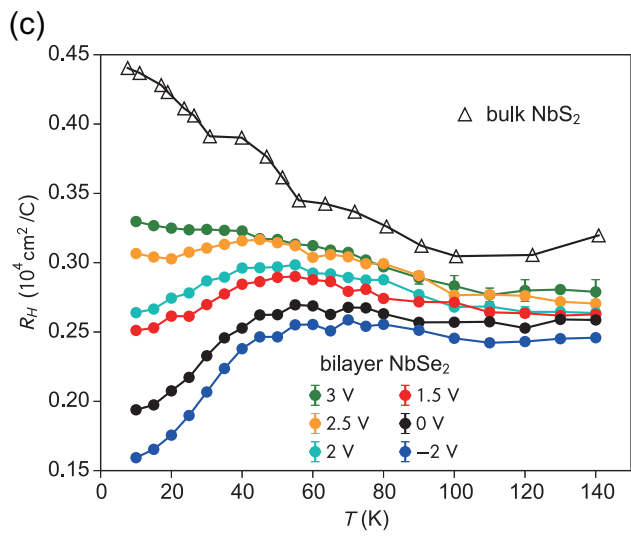
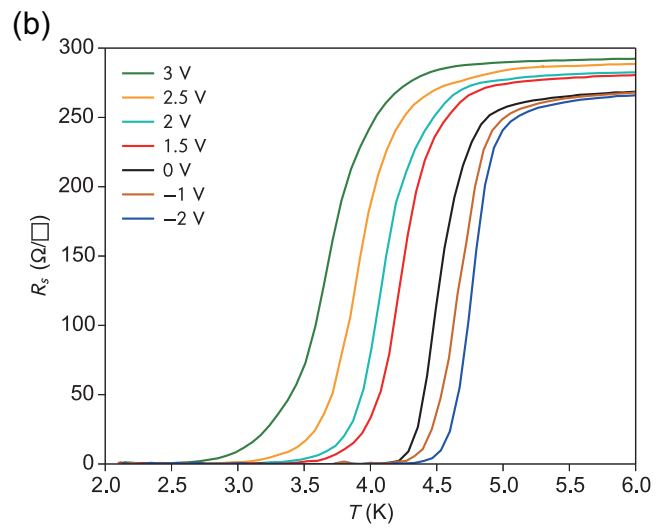
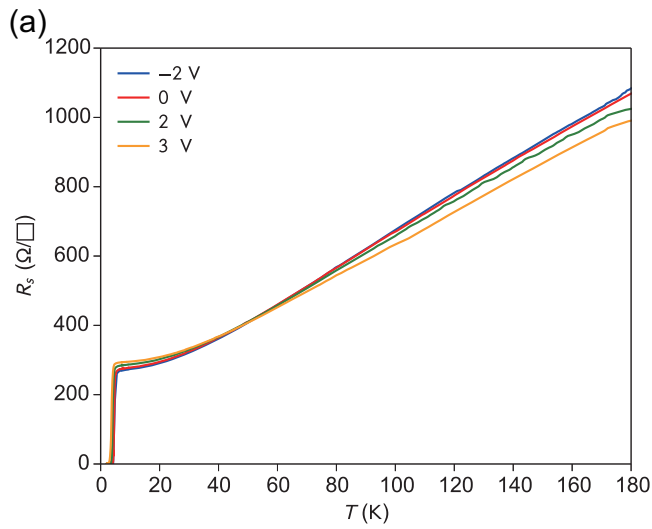
FIG. 2. (a-c) Temperature dependence of the longitudinal sheet resistance (a, b) and the sheet Hall coefficient (c) at selected gate voltages. Longitudinal sheet resistance across

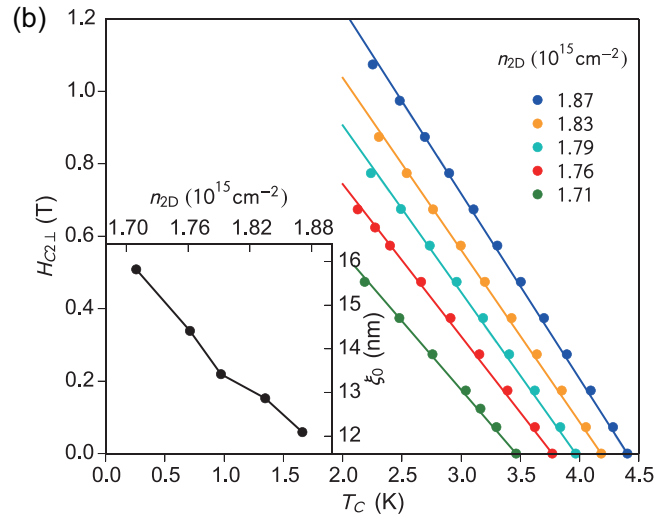
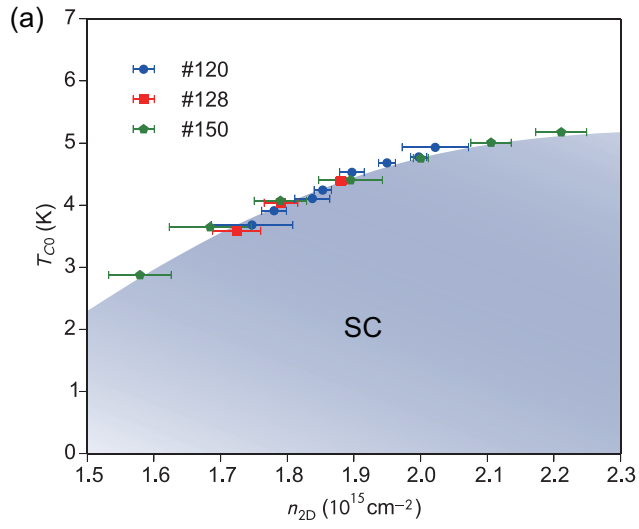
the superconducting transition is shown in (b). Data from bulk NbS₂ [44] are also shown as empty triangles in (c). (d) Gate voltage dependence of the sheet carrier density. The error bars are estimated from the uncertainties in the sheet Hall coefficient. The dashed line is a linear fit. All data are from device #120.

FIG. 3. (a) T_{C0} - n_{2D} phase diagram of bilayer NbSe₂. The horizontal error bars originate from the measurement uncertainty of the Hall coefficient. The filled area corresponding to the superconducting (SC) phase is a guide to the eye. (b) $H_{C2\perp}$ - T_C phase diagram of bilayer NbSe₂ under a magnetic field perpendicular to the sample at different doping levels. The symbols are T_C determined as the temperature corresponding to 50% of the normal state resistance. The lines are linear fits. The inset shows the carrier density dependence of the zero-temperature coherence length extracted from the linear fits.

FIG. 4. (a) Dimensionless e - ph coupling constant as a function of sheet carrier density. The vertical and horizontal error bars are from fitting of the normal-state resistance to the e - ph scattering model and the measurement uncertainty of the Hall coefficient, respectively. (b) Superconducting transition temperature T_{C0} as a function of e - ph coupling constant λ for bilayer NbSe₂. The solid line is the best fit to the strong-coupling formula [Eq. (1)] with $\omega_{log} = 50$ K and $\mu^* = 0.10$.







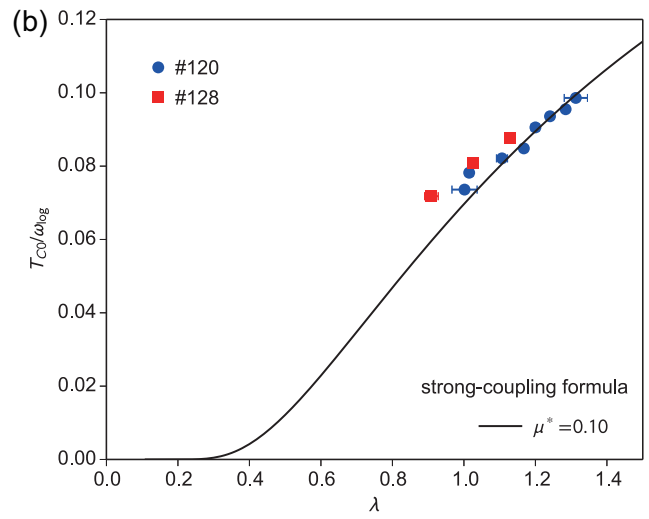
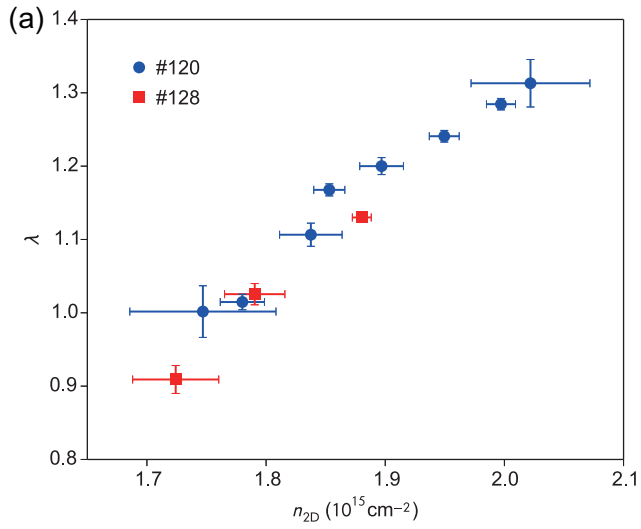


Figure 4 LR15126 01AUG2016